International Journal of Fluid Machinery and Systems
Vol. 7, No. 2, April-June 2014

DOI: http://dx.doi.org/10.5293/IJFMS.2014.7.2.060
ISSN (Online): 1882-9554

Original Paper

Effect of Inlet Geometry on Fan Performance and Inlet Flow Fields in a Semi-opened Axial Fan

Pin Liu[1], Norimasa Shiomi[1], Yoichi Kinoue[1], Toshiaki Setoguchi[1] and Ying-zi Jin[2]

[1]Department of Mechanical Engineering, Saga University
1 Honjo-machi, Saga, 840-8502, Japan, liupinsky@163.com, siomi@me.saga-u.ac.jp, kinoue@me.saga-u.ac.jp, setoguci@me.saga-u.ac.jp
[2]Institute of Mechatronics, Zhejiang Sci-Tech University
Xiasha Higher Educational Zone, Hangzhou, 310018, P. R. China, Jin.yz@163.com

Abstract

In order to clarify the effect of inlet bellmouth size of semi-opened type axial fan on its performance and flow fields around rotor, fan test and flow field measurements using hotwire anemometer were carried out for 6 kinds of bellmouth size. As results of fan test, the shaft power curve hardly changed, even if the bellmouth size changed. On the other hand, the pressure-rise near best efficiency point became small with the bellmouth size decreasing. Therefore, the value of maximum efficiency became small as the bellmouth size decreased. As results of flow field measurements at fan inlet, the main flow region with large meridional velocity existed ne ar blade tip when the bellmouth size was large. As bellmouth size became smaller, the meridional velocity at fan inlet became smaller and the one at outside of blade tip became larger. As results of flow field measurem ents at fan outlet, the main flow region existed near rotor hub side.

Keywords: Fan, semi-opened, inlet geometry, measurement.

1. Introduction

Semi-opened axial fan is the fan that it doesn't have the duct at upstream and downstream of fan. It has only the casing at blade tip region. In this, one part of rotor blade tip is covered with casing and another part is opened. As the structure of fan is simple and the flow-rate of fan is relatively large, so its fan is often used as home products, e.g. room ventilation fan, cooling fan of outdoor unit of air conditioner, and so on. Recently, from the viewpoint of energy saving and quiet surrounding in house, it has been strongly desired to be high performance and low noise level also about these fans. Therefore, the researches for these fans are gradually increasing [1]-[6].

As the place which can be attached is limited for these fans, the size of fan such as axial length and tip diameter is restricted in many cases. The semi-opened type is the one of them. The shape of rotor blade of semi-opened fan is long chord length at blade tip and short at blade hub. It means that the main work is done at blade tip side. When a part of blade tip region is opened and the radial inflow from its region occurs, radial inflow and axial inflow interfere for each other at the region near blade tip. As a result, a large loss is caused and the fan performance becomes low. On the other hand, as a part of blade tip region is opened, it is possible to suck air into fan from a large area by a radial direction. It is desirable performance as a ventilation fan.

The spatial restriction also brings about the restriction for casing geometry. In many case, the bellmouth is equipped at fan inlet to suck air in fan smoothly. For semi-opened fan, the bellmouth and casing are formed by one. It is, therefore, considered that the effect of bellmouth size and geometry on fan performance is very large. It is very important to clarify the effect of them, but the researches for them are not so many [7, 8].

The final gold of this investigation is to establish the design method to make high performance semi-opened fan. As the first step for reaching this goal, the experimental investigation was carried out to clarify the effect of inlet bellmouth size on fan performance and flow fields around fan.

Received March 12 2013; accepted for publication April 15 2014: Review conducted by Prof. Yoshinobu Tsujimoto. (Paper number O13020J)
Corresponding author: Norimasa Shiomi, Professor, siomi@me.saga-u.ac.jp

2. Experimental Apparatus and Procedure

Fig.1 shows the schematic view of test rig and its component list. The section geometry of the test rig is rectilinear and its size is 880mm x 880mm. The flow direction is left to right in Fig.1. As the test rig didn't have the throttle to change the flow-rate, the flow-rate was changed by changing the power of booster fan. At the fan test, the pressure-rise in the box, shaft power and the pressure difference at nozzle were measured for each flow-rate condition. The rotor blade location at hotwire survey was detected by use of photo sensor mounted on motor shaft.

Fig.2 shows the outline of the test rotor. The rotor has 5 blades, its tip diameter is approximately 180mm, and the hub-to-tip ratio is approximately 0.51.

Fig.3 shows the outline of test fan with casing and bellmouth on meridional plane. A rear half of blade tip is fully covered with casing and the tip clearance is 1mm at constant. A front half of blade tip is opened and 6 types of circular-arc bellmouth including the case of no bellmouth are set here. The radius of inlet bellmouth, R, is 25mm, 20mm, 15mm, 10mm, 5mm, and 0mm (without bellmouth), respectively. In this study, it is called as R25, R20, R15, R10, R05, and R00, respectively.

The hotwire survey location is also shown in Fig.3. In this, "RF" means "Rotor Front" survey line, "RO" means "Rotor Outside" survey line, and "RR" means "Rotor Rear" survey line. "RF" and "RR" are survey lines common to all types of inlet bellmouth. On the other hand, the number of "RO" survey line changes with bellmouth R size, that is, the number of "RO" survey line is 0 in case of R25 and it is 5 in case of R00. The radial measurement stations are 17 points on RF, 9 points on RO and 15 points on RR. The "r08" on RF survey line corresponds with blade tip location at blade leading edge and the "r13" on RR survey line corresponds with it at blade trailing edge.

A single I-type hotwire probe was used at the measurement of RF and RO. The orientation of hotwire probe was two directions. One was the direction normal to meridional plane and the other was the one parallel to meridional plane. In case of normal to meridional plane, the velocity component measured includes both radial and axial velocity component, so it is called as "V_{ar}" velocity component in this study. In case of parallel to meridional plane, it includes both radial and tangential velocity component, so it is called as "V_{tr}". The measurement data were phase-locked averaged using rotor rotating signal from photo sensor.

A single slanted hotwire probe was used at the measurement of RR. Its probe was rotated about its axis at the interval of 7.2 degrees in the range of 180 degrees. The data were processed by the use of periodical multi sampling technique, and the velocity wad divided into axial, tangential and radial velocity component. However, as the measurement range was limited in 180 degrees, the reversed flow was not captured in this study. It is a future (next) subject.

The rotor rotating speed is 3,000 (min^{-1}) at constant. The test Reynolds number based on the blade tip speed and blade chord length at mid-span is 1.32×10^5

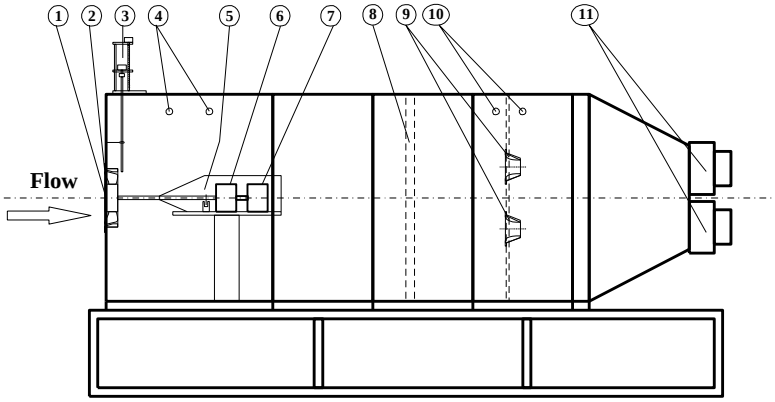

1	Test rotor
2	Casing
3	Hotwire traverse
4	Pressure taps
5	Photo sensor
6	Torque meter
7	Motor
8	Gauge screen
9	Nozzles
10	Pressure taps
11	Booster fan

Fig. 1 Schematic view of test rig and its component list

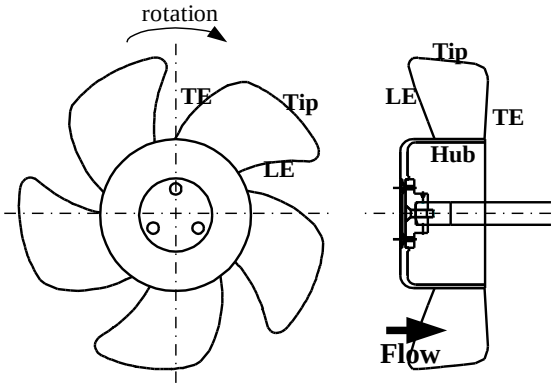

Fig. 2 Outline of test rotor

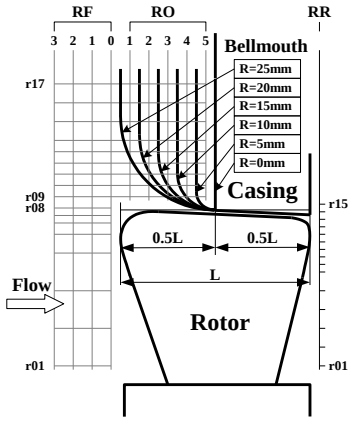

Fig. 3 Outline of test fan with 6 types of bellmouth and hot-wire survey lines and stations

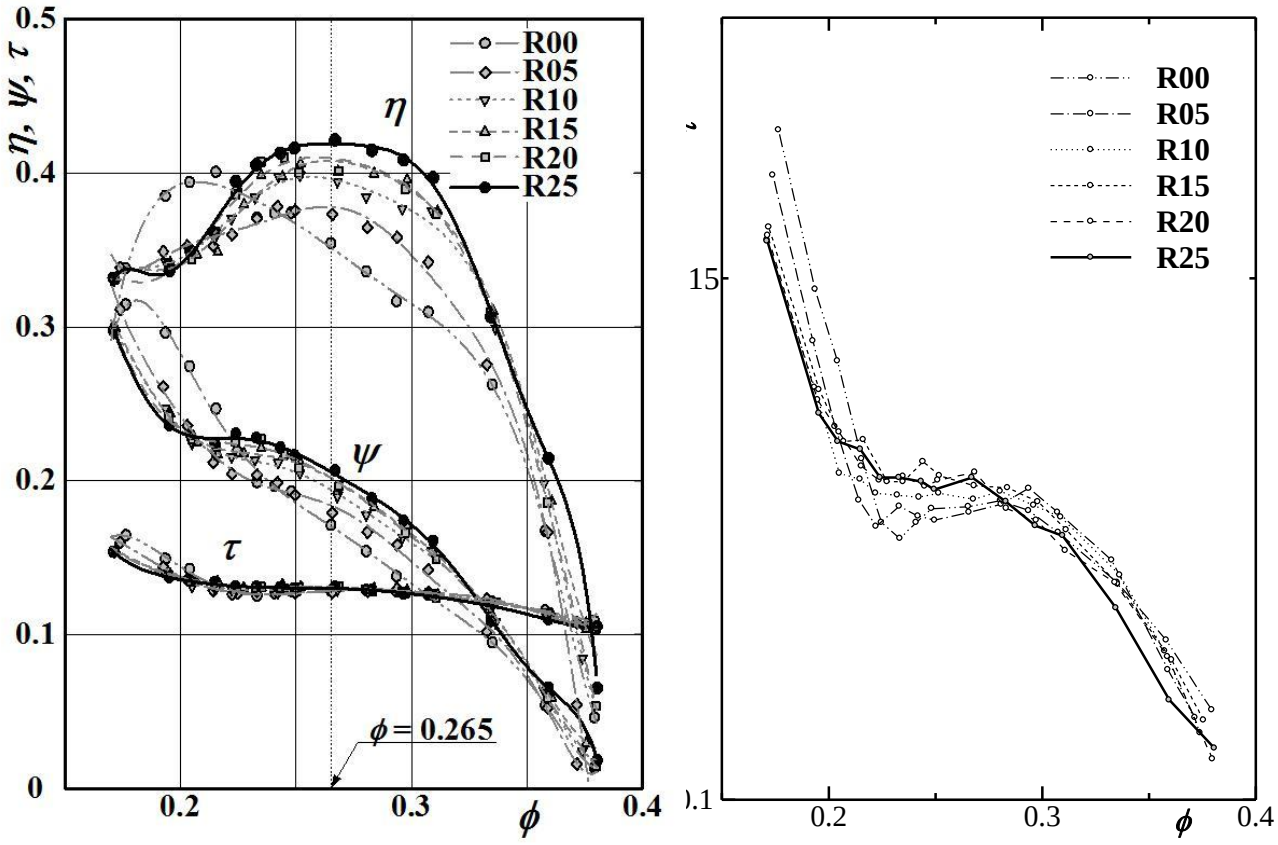

Fig. 4 Characteristic curves of test fan for 6 types of inlet bellmouth size

3. Experimental Results and Discussion

3.1 Fan Test Result

Fig.4 shows the result of fan test for 6 types of inlet bellmouth. At the left-side figure, the abscissa is flow-rate coefficient, ϕ, and the ordinate is efficiency, η, pressure-rise coefficient, ψ, and torque coefficient, τ. The symbols in figure correspond with the type of inlet bellmouth. At the right-side figure, the torque curves are enlarged because its changes are very small at the left-side figure.

It is found that the pressure-rise coefficient drops at the region of $\phi > 0.2$ when the size of bellmouth radius is small, although the torque coefficient is almost the same for all types. Observing the torque curses in detailed, torque coefficient at large flow rate region becomes small in case of larger bellmouth size. The stall point, which means the local maximum point on pressure-rise curve, shifts to higher flow-rate region and it becomes less apparent gradually. In case of R05, the stall point disappears. As a result from them, efficiency drops as the size of bellmouth radius is smaller. Maximum efficiency was obtained at $\phi = 0.265$ in case of R25 and its value is approximately 42%. The flow-rate where the maximum efficiency was obtained was almost the same, except for the case of R00.

Form the pressure-rise curve, the pressure tends to gradually drops until the case of R15, and after then it drops rapidly.

The flow field measurements were carried out at 4 flow-rate conditions; those are $\phi = 0.265$ (reference), $\phi = 0.320$ (large flow-rate), $\phi = 0.230$ (near stall) and $\phi = 0.210$ (in stall).

3.2 Effect of Inlet Geometry on Circumferentially Averaged Velocity Fields at Fan Inlet

Fig.5 (a)(b)(c) and Fig.6 (a)(b)(c) show the contour maps of circumferentially averaged V_{ar} and V_{tr} velocity component on meridional plane at reference flow condition, $\phi = 0.265$. Figure (a) for both fig.5 and fig.6 is a result in case of R25, Figure (b) is in case of R15, and Figure (c) is in case of R05. The abscissa for each figure is axial direction and the ordinate is radial direction, respectively. In this, r^* is non-dimensional radius normalized by the blade span and the "$r^* = 1.0$" indicates blade tip location at blade leading edge. The flow direction is from left to right. Each velocity value is non-dimensional velocity normalized by blade tip speed.

Before the hotwire survey was done, a simple flow visualization using simple tuft was carried out at RF and RO locations (The photo is left out). As a result, it was found that the tangential velocity component at RO location was almost zero except for the region near blade tip and the radial velocity component at RF and $r^* < 1.0$ location was almost zero, too. These results are considered in the following discussion.

In case of R25 shown in Fig.5(a), the value of V_{ar} becomes large near blade leading edge at the region from $r^* = 0.5$ to 1.0 on RF0 and it becomes gradually small at the region away from blade leading edge. The air smoothly flows into the fan along bellmouth wall. The velocity distribution exists even where r^* is relatively large region. When the R size of bellmouth becomes small, the axial inflow decreases and the radial inflow increases.

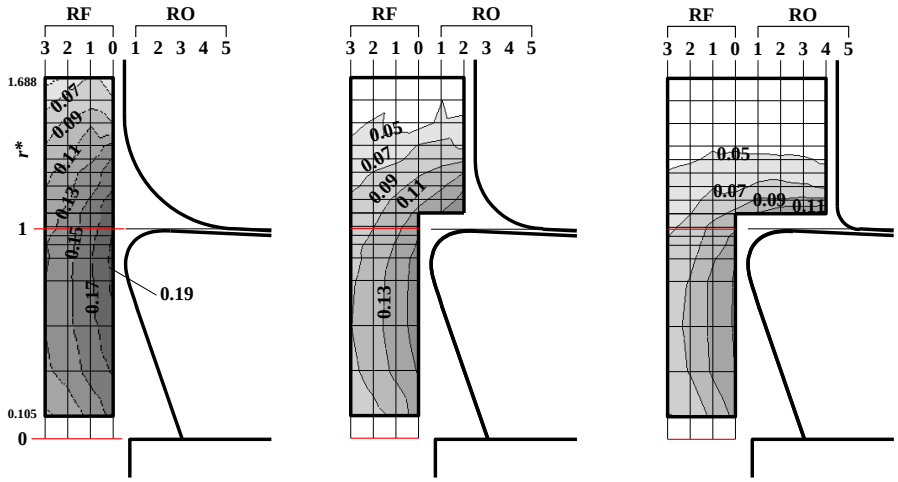

(a) R25 (b) R15 (c) R05

Fig. 5 Contour maps of circumferentially averaged V_{ar} at fan inlet at ϕ = 0.265

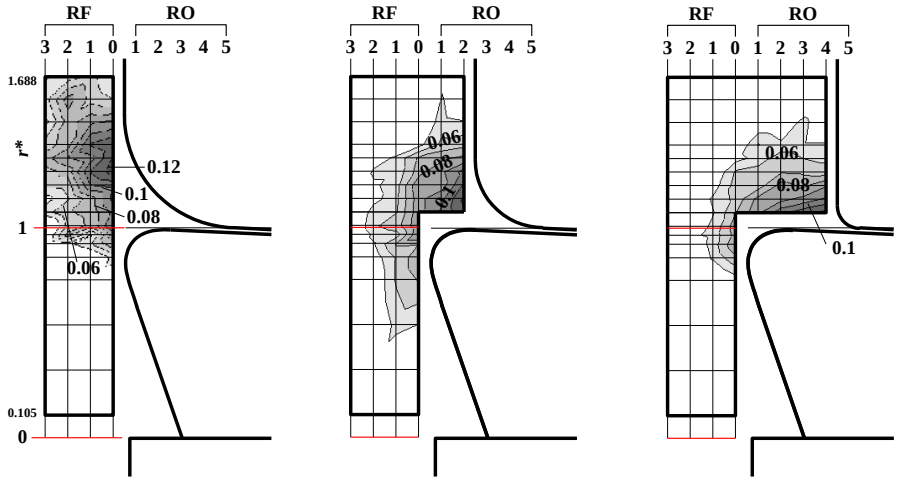

(b) R25 (b) R15 (c) R05

Fig. 6 Contour maps of circumferentially averaged V_{tr} at fan inlet at ϕ = 0.265

In case of R25 shown in Fig.6(a), the value of V_{tr} becomes large near the location of r* =1.3 to 1.4, in which the bellmouth radius start, on RF0. It means that the air smoothly flows into the fan along bellmouth wall. The value of V_{tr} is very small at the location of $r^* < 1.0$, so it is found that the velocity component in this region is almost the axial velocity component. When the R size of bellmouth becomes small, the large velocity region for V_{tr} is limited near blade leading edge and blade tip. Compared the velocity in front of rotor, the velocity at outside of rotor is large.

From these results, the change of overall flow tendency with changing the R size of bellmouth is shown. The increase of radial inflow causes the performance drop because the blockage area is formed by flow mixing between radial and axial inflow.

3.3 Effect of Inlet Geometry on Phase-locked Averaged Velocity Fields at Fan Inlet

Fig.7 (a)(b) and Fig.8(a)(b) show the contour maps of phase-locked averaged V_{ar} and V_{tr} velocity component on r-θ plane at RF0 location at reference flow condition, ϕ = 0.265. Fig.7 is the result for R25 and Fig.8 is the result of R05. The abscissa is pitchwise direction and the ordinate is radial direction. The bold line in figure indicate the blade leading edge line and the blade rotating direction is from left to right, as shown in figure. The symbol "PS" and "SS" indicate the blade pressure surface and suction surface, respectively.

In the case of R25 shown in Fig.7, as it is found from simple visualization that radial velocity is almost the zero at this flow-rate condition at the region of $r^* < 1.0$ except for the region near blade, the high velocity region ($V_{ar} > 0.21$) observed on blade SS side near blade tip ($r^* = 1.0$) in Fig.7 (a) indicates axial inflow (It is called as axial main flow region after then). Also, as it is found from simple visualization that tangential velocity is almost zero at this flow-rate condition at the region of $r^* > 1.0$ except for the region near blade, the high velocity region ($V_{tr} > 0.09$) observed outside of blade tip ($r^* > 1.0$) at blade mid-pitch in Fig.7 (b) indicates the radial inflow (It is called as radial main flow). In the Fig. 7(b), the small high velocity region on blade SS side near blade tip ($r^* = 1.0$) exists. As this region is, however, close to the blade, it needs that the V_{tr} velocity component is divided into V_t and V_r velocity component in order to discuss the flow in this region.

In case of R05 shown in Fig.8, the value of axial main flow region shown in Fig.8 (a) becomes small compared with the result in case of R25, but the distribution of it is similar to the result in case of R25, that is, the axial main flow region is formed on blade SS side near blade tip and expanded toward blade mid-pitch. It means that the flow-rate of axial inflow decreases. The velocity distribution outside of blade tip ($r^* > 1.0$) differs compared with the result in case of R25. It is considered that the casing

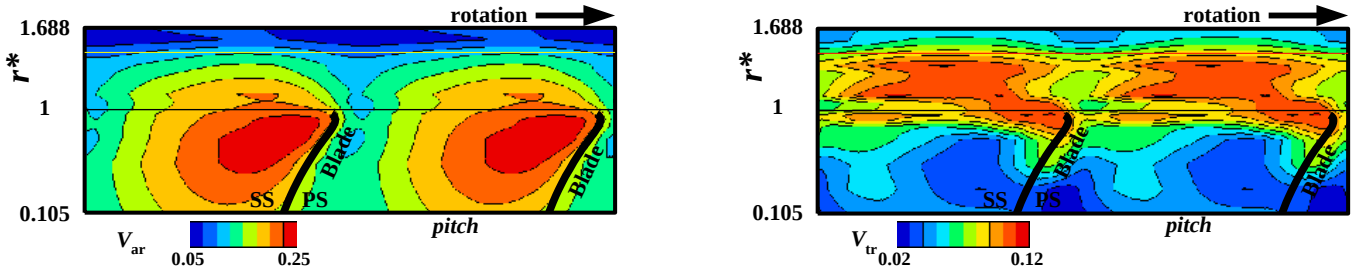

(a) V_{ar} component (b) V_{tr} component

Fig. 7 Contour maps of phase-locked averaged velocity on RF0 plane at ϕ = 0.265 in case of R25

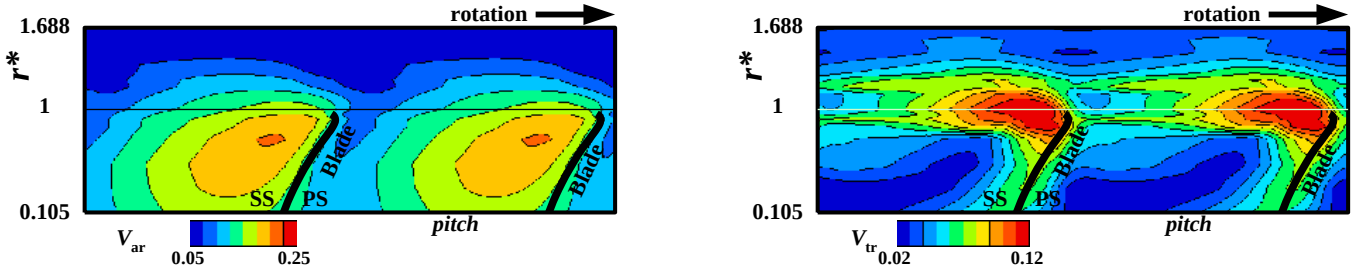

(a) V_{ar} component (b) V_{tr} component

Fig. 8 Contour maps of phase-locked averaged velocity on RF0 plane at ϕ = 0.265 in case of R05

wall normal to rotor axis shifts to downstream side as the bellmouth size becomes small, that is, the effect of the wall on flow field decreases. This effect is more clearly observed at the result of V_{tr} velocity distribution shown in Fig.8 (b). The radial main flow region observed in Fig.7 (b) is not observed in Fig.8 (b), while locally high velocity region near blade tip on blade SS side exists similar to the result of Fig.7 (b) and its region is extending toward mid-pitch. It is, therefore, found that the wall normal to rotor axis has not affected this locally high velocity region, that is, this region is formed by the suction flow on blade SS side near blade tip.

3.4 Effect of Inlet Geometry on Phase-locked Averaged Velocity Fields at Fan Outlet

Figs.9&10 show the contour maps of the axial and circumferential velocity at rotor outlet, respectively. Fig.11 shows the contour maps of velocity fluctuations at rotor outlet. Figure (a) is the result in case of R25 and figure (b) is the result in case of R05. The abscissa is pitch-wise direction and the ordinate is radial direction, respectively. The bold solid line indicate the blade trailing edge and its rotating direction is from left to right as shown in figure. The color legend indicates the non-dimensional velocity normalized by the blade tip speed.

The main flow region is relatively radial inward region for both cases of R25 and R05 and the low velocity region is formed near blade tip on blade PS side. The velocity distribution for each figure is similar, but the value of main flow region differs even if the flow-rate condition is the same. It is thought that the low velocity region near blade tip on blade PS side in case of R05 is reversed flow region in order to fulfill the condition that the flow-rate is the same. As it was not, however, considered that the reversed flow region was formed at this flow-rate condition, the measurement detecting the reversed flow region was not conducted. Now, it is the future work. On the other hand, the circumferential velocity in case of R25 is totally larger than the one in case of R05. It means that the Euler head of R25 is larger than the one of R05. Therefore, the pressure-rise of R25 is bigger than the one of R05.

As the velocity fluctuation in case of R05 is compared with the one in case of R25, the velocity fluctuation in case of R05 becomes larger for magnitude and area. From the results of axial velocity distributions, the low velocity regions are formed near blade tip on blade PS and in this region the separation occurs. The degree of separation in case of R05 is stronger than the one in case of R25.

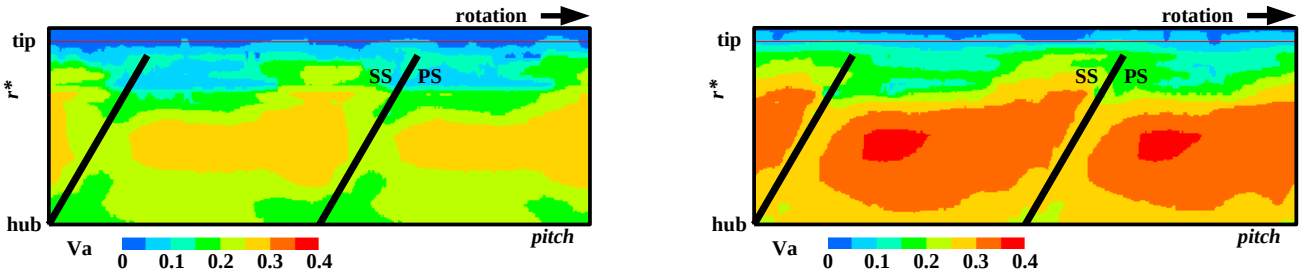

(a) In case of R25 (b) In case of R05

Fig. 9 Contour maps of phase-locked averaged axial velocity at rotor outlet at ϕ = 0.265

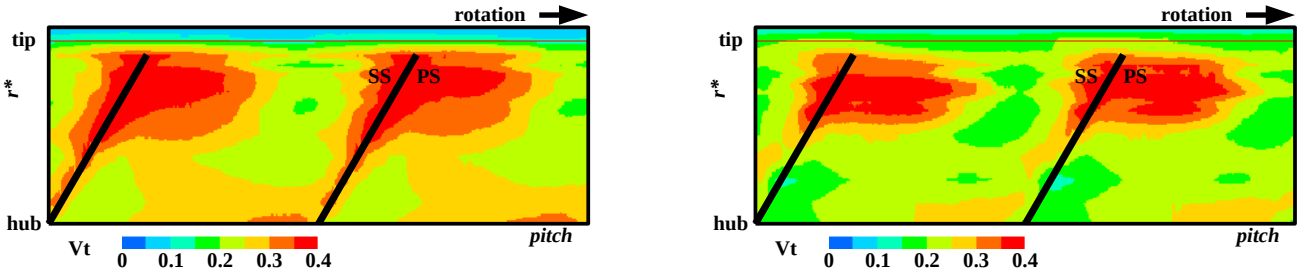

(a) In case of R25 (b) In case of R05

Fig. 10 Contour maps of phase-locked averaged circumferential velocity at rotor outlet at $\phi =$ 0.265

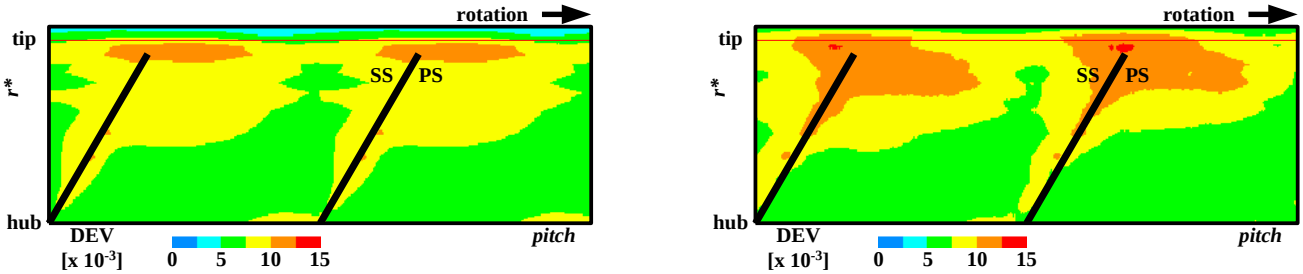

(a) In case of R25 (b) In case of R05

Fig. 11 Contour maps of phase-locked averaged velocity fluctuations at rotor outlet at $\phi =$ 0.265

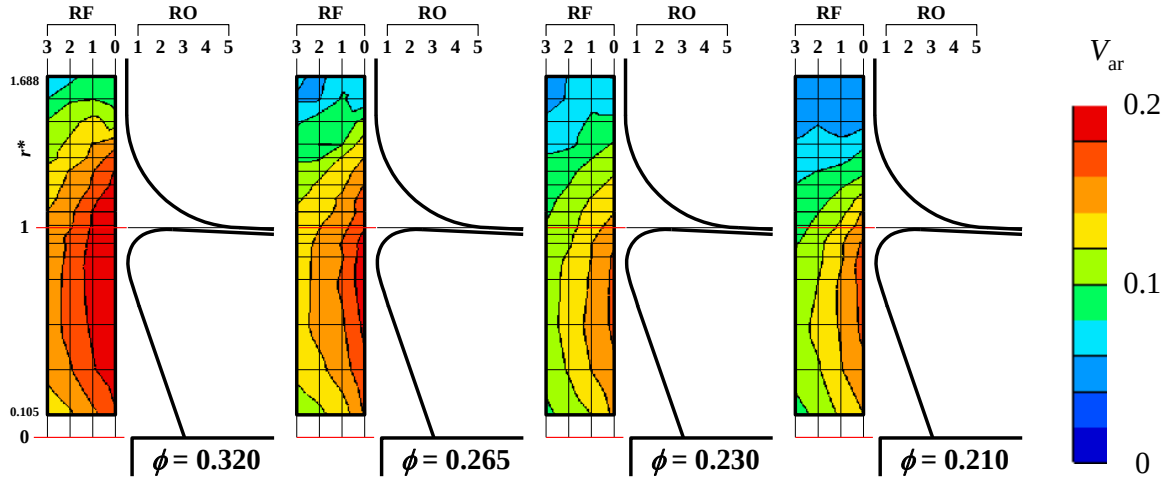

(a) Distributions of velocity for V_{ar} component

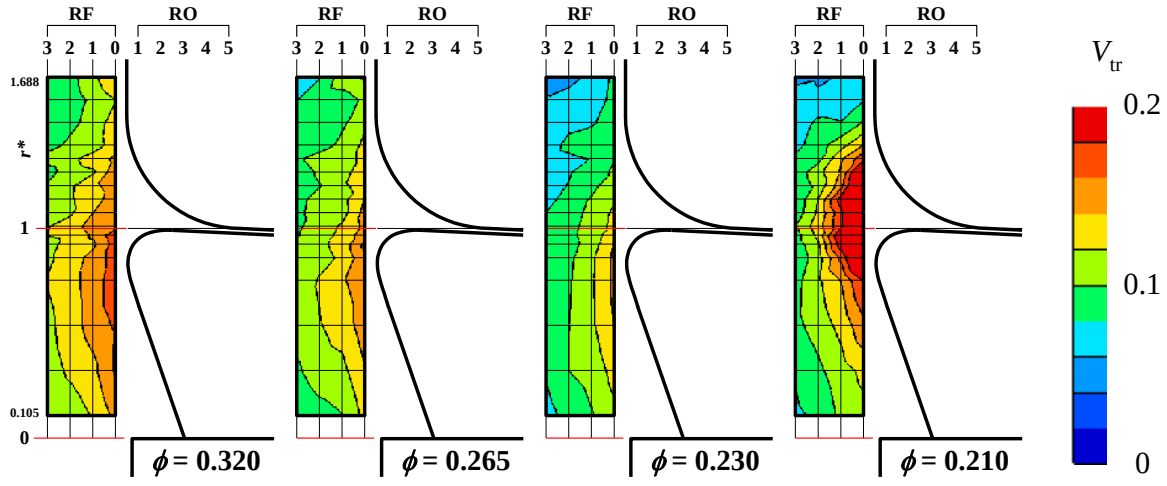

(b) Distributions of fluctuation for V_{tr} component

Fig. 12 Contour maps of circumferentially averaged velocity and its fluctuations at rotor inlet in case of R25

3.5 Effect of Flowrate on Circumferentially Averaged Velocity Fields at Fan Inlet

Fig.12 (a)(b) show the contour maps of circumferentially averaged V_{ar} (Fig.12 (a)) and its deviations (Fig.12 (b)) at fan inlet for four flow-rate conditions in case of R25. The abscissa of all figures is axial direction and the ordinate is non-dimensional radius, r^*, respectively. The value on ordinate is normalized by the blade span height and r^*=1.0 is corresponding to blade tip. The red color in these figures indicates high value and blue color indicates low value, respectively. The left end figure is a result in case of ϕ = 0.320. It takes for going to the right figure and the flow-rate decreases with ϕ = 0.265, 0.230, and 0.210.

For the results of velocity, the main flow region with large velocity concentrates on the front of blade leading edge in all cases. The value of maximum velocity decreases and the main flow region reduces as the flow-rate becomes small. However, it seems that the results of ϕ = 0.230 and 0.210 is almost the same.

For the results of deviation, the region with high velocity deviation is almost corresponding to the one with large velocity except for the result of ϕ = 0.210. Its value becomes low and the area with high velocity deviation reduces as the flow-rate becomes small. The velocity deviation, however, rapidly increases in case of ϕ = 0.210. The location of the region with high

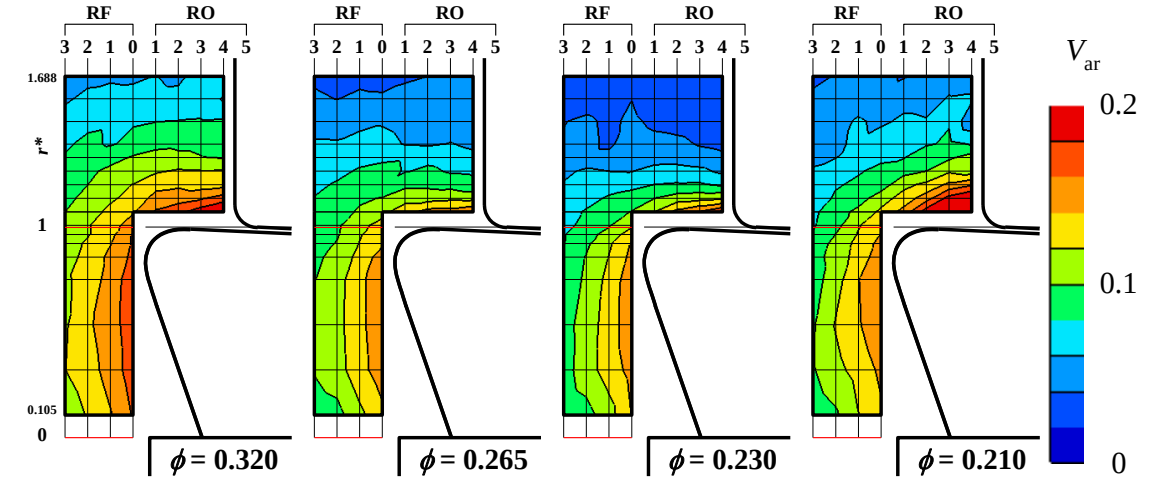

(a) Distributions of velocity for V_{ar} component

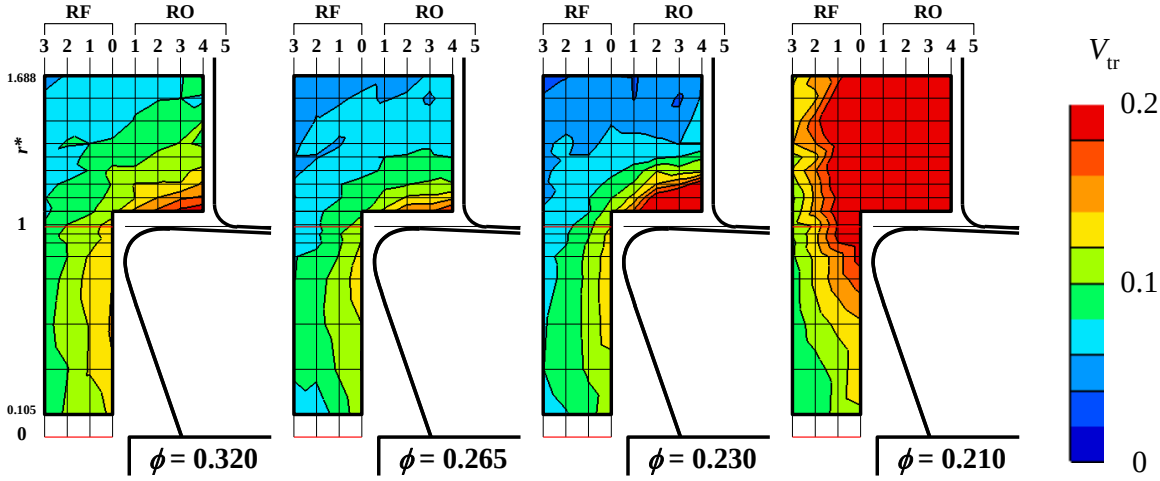

(b) Distributions of fluctuation for V_{tr} component

Fig. 13 Contour maps of circumferentially averaged velocity and its fluctuations at rotor inlet in case of R05

deviation is not corresponding to the one with large velocity. Its location exists around blade tip (near r^* =1). Corresponding to the results of ϕ = 0.230 and 0.210, the distribution of velocity is almost the same one, but the distribution of deviation completely differs by them. It means that the blade has been stalled near blade tip, and it is considered that the reversed flow from rotor blade with blade stall have caused the increase of deviation.

From the above results, it is found in case of R25 that the blade stall occurs at the flow condition between ϕ = 0.230 and 0.210, and the effect of blade stall on flow field is mainly observed near blade tip region.

Fig. 13 (a)(b) show the contour maps of circumferentially averaged velocity and its deviations at fan inlet in case of R05. The view of the figures is the same as Fig.12.

The main flow region decreases with changing flow-rate from ϕ = 0.320 to 0.265. However, it does not change when the flow-rate decreases from ϕ = 0.265 to 0.230. As the flow-rate more decreases from ϕ = 0.230 to 0.210, the value of maximum V_{ar} becomes large and the area with large velocity extends especially to the region outside of blade tip.

For the results of deviation, the velocity deviation at the location outwards of blade tip rapidly increases between ϕ = 0.265 and 0.230. Its reason is due to blade stall and the interference of the radial inflow and recirculation zone formed by blade stall

occurs near blade tip. As the flow-rate more decreases to $\phi = 0.210$, the deviation at outside of blade tip extremely increases for its value and its area. The area with high velocity deviation expands to the region ahead of rotor.

From the above results, it is found in case of R05 that the blade stall occurs at the flow condition between $\phi = 0.265$ and 0.230, and the effect of blade stall on flow field is mainly observed at the location outwards of blade tip.

4. Conclusions

In order to clarify the effect of inlet bellmouth size on fan performance and flow fields around fan, the fan test and hotwire measurements were carried out in a semi-opened axial fan and the changes of fan characteristics and flow fields were clarified. Furthermore, it is also clarified how the flow condition changes for each bellmouth size when the flow-rate is changed.

The larger inlet bellmouth size is desirable, but it is possible to make bellmouth size small to some extent. When the bellmouth size becomes small, the shaft power is almost the same value and distribution. On the other hand, the pressure-rise characteristic drops with decreasing the bellmouth R size.

When the bellmouth size becomes small, the axial main flow decrease and radial main flow increases. As the result, flow interaction near blade tip is strengthened and the fan performance is reduced. At rotor outlet, the main flow region shifts to radial inward below the blade mid-span for all bellmouth sizes.

Also, when the bellmouth size becomes small, the blade stall occurs at higher flow-rate. The region affected by blade stall is observed at the location ahead of rotor in case of R25 at $\phi = 0.210$, while it is observed at the one radial outside of blade tip in case of R05 at $\phi = 0.230$. As the flow-rate decreases up to $\phi = 0.210$ in case of R05, the velocity deviation at the region radial outwards of blade tip violently increases for its value and the area with high velocity deviation greatly expands.

Nomenclature

DEV	Velocity fluctuation [-]	V_{ar}	Non-dimensional resultant velocity for axial and radial direction (= V/U_t)
PS	Indicate blade pressure surface	V_{tr}	non-dimensional resultant velocity for tangential and radial (= V/U_t)
r^*	Non-dimensional radius (=$r/(r_t - r_h)$)	U_t	Blade tip speed [m/s]
r_h	Hub radius [m]	ϕ	Flow-rate coefficient
r_t	Tip radius [m]	η	Efficiency
R	Indicate bellmouth radius	τ	Torque coefficient
RF	Indicate rotor front	ψ	Pressure-rise coefficient
RO	Indicate outside of rotor tip		
SS	Indicate blade suction surface		

References

[1] T. Shigemitsu, J. Fukutomi and T. Agawa, 2013, "Internal Flow Condition of High Power Contra-Rotating Small-Sized Axial Fan," International Journal of Fluid Machinery and Systems, Vol. 6, No. 1, pp. 25-32.

[2] N. Shiomi, Y. Kinoue, T. Setoguchi and K. Kaneko, 2011, "Vortex Features in a Half-ducted Axial Fan with Large Bellmouth (Effect of Tip Clearance)," International Journal of Fluid Machinery and Systems, Vol. 4, No. 3, pp. 307-316.

[3] L. Zhu, Y.-Z. Jin, Y. Li, Y. Jin, Y. Wang and L. Zhang, 2013, "Numerical and Experimental Study on Aerodynamic Performance of Small Axial Flow Fan with Splitter Blades," Journal of Thermal Science, Vol. 22, No. 4, pp. 333-339.

[4] S. Sasaki, I. Torise, H. Hayashi, 2012, "An Experimental and Numerical Study on Wake Vortex Noise of a Low Speed Propeller Fan," Open Journal of Fluid Dynamics, Vol. 2012, pp. 290-296.

[5] T. Shigemitsu, J. Fukutomi, and Y. Okabe, 2010, "Performance and Flow Condition of Small-Sized Axial Fan and Adoption of Contra-Rotating Rotors," Journal of Thermal Science, Vol. 19, No. 1, pp. 1-6.

[6] N. Shiomi, Y. Kinoue, Y.-Z. Jin, T. Setoguchi and K. Kaneko, 2009, "Flow Fields with Vortex in a Small Semi-open Axial Fan," Journal of Thermal Science, Vol. 18, No. 4, pp. 294-300.

[7] M. Arai, T. Ishima, T. Obokata, 2003, "PIV Measurement and Numerical Prediction of Flow around a Fan : Effects of Bellmouth Shape and Position," Visualization, Suppl. 23(1), pp. 203-206. (in Japanese)

[8] Pin Liu, Norimasa Shiomi, Yoichi Kinoue, Ying-zi Jin, Toshiaki Setoguchi, 2012, "Effect of Inlet Geometry on Fan Performance and Flow Field in a Half-Ducted Propeller Fan," International Journal of Rotating Machinery, Vol. 2012, Article ID. 463585.